Nanotechnology Perceptions
ISSN 1660-6795
www.nano-ntp.com

Investigating the Impact of Thermal Radiation and Convective Heating on Casson Fluid Flow with Cattaneo-Christov Heat Flux Model: Using the Keller Box Method

K. Keziya[1], Ch. Suresh kumar[2], Y. Devasena[3*], P. D. Selvi[4], A. Shobha[4], Sd. Abdul Khadar Jilani[5]

[1]Department of Mathematics, DS Govt. Degree College (W), Ongole, Andhra Pradesh, India
[2]Department of Mathematics, KRK Govt. Degree College, Addanki, Andhra Pradesh, India
[3]Department of Basic Sciences and Humanities, School of Engineering and Technology, Sri Padmavati Mahila Visvavidyalayam, Tirupati, Andhra Pradesh, India, Yellamraju.devasena@gmail.com
[4]Department of Applied Mathematics, Sri Padmavati Mahila Visvavidyalayam, Tirupati, Andhra Pradesh, India.
[5]Department of Mathematics, Govt. Degree College, Cumbum, Andhra Pradesh, India.

This paper presents an analysis of boundary layer flow for a Casson fluid model, accounting for thermal radiation and convective heating effects near a stretching sheet with variable thickness. The heat transfer process is examined using the Cattaneo-Christov heat flux model, an improved version of Fourier's law. To simplify the problem, the governing partial differential equations are transformed into nonlinear ordinary differential equations through appropriate similarity transformations. The numerical solution is derived using the Keller-Box method. The study focuses on various physical quantities of interest with respect to key influential parameters. It is observed that the velocity profile decreases as the Casson fluid parameter increases. Additionally, the results show that the temperature distribution diminishes with increasing thermal relaxation factor values, while it rises with greater thermal radiation factor values.

Keywords: Thermal radiation, Casson fluid, Cattaneo- Christov Heat flux model, convective heating, Keller box method.

1. Introduction

In the production of polymer sheets, achieving the desired thickness involves stretching the melted sheet emitted from a slit. This process is intricate and requires careful consideration of multiple parameters to optimise the final product's quality and properties. Researchers and engineers delve into understanding the dynamics of boundary layer flow to enhance the efficiency and effectiveness of these manufacturing processes. The cooling rate during stretching plays a crucial role in determining the molecular structure and mechanical properties of the polymer sheet. A controlled cooling process ensures that the sheet maintains the desired characteristics, such as strength and flexibility. Additionally, the stretching rate, which influences the orientation and alignment of polymer chains, directly affects the sheet's mechanical and thermal properties.

In the realm of glass fibre manufacturing, metallic sheet cooling, polymer sheet extraction from dye, paper production, and petroleum resource improvement, advancements in the assessment of boundary layer flow contribute to more efficient and sustainable engineering practices. This interdisciplinary approach, combining fluid dynamics, thermodynamics, and material science, fosters innovation and progress in diverse industrial applications. Crane [9] explained for the first time that the boundary layer flow is provoked by a linearly stretching sheet. Gupta and Gupta [13] extended the classical problem by Crane [9] to a porous stretching surface and assumed that the velocity of the sheet may not conform to be linear, which leads to the investigation of the problem of stretching sheet. Ali [1] inspected viscous fluid boundary layer flow upon non-linearly stretching sheet. Cortell [8] carried out the effort of Ali [1] by considering both prescribed surface temperature and constant surface temperature through the sheet. Kechil and Hashim [19] investigated a chemical reaction effect over a viscous fluid past a non-linearly stretching sheet around a porous medium.

Constitutive equations of differential type fluids are simple about velocity components. The literature survey designates that slight focus has been given to the flow of fluids of rate type. The Fluid model by Casson is one among the non-Newtonian fluid models which disclose the features of yield stress. Further Casson fluid moves if the applied shear stress is greater than the yield stress and behaves like a solid when the shear stress is less than the yield stress [11, 24, 25, 23 and 35]. Honey, jelly, tomato sauce, vigorous fruit juices, soup are some of the examples of Casson fluid.

One of the essential mechanisms in the investigation of boundary layer flow of Newtonian and non-Newtonian fluids is the convective boundary condition at the boundary wall. Aziz and Makinde [23] scrutinise numerically boundary layer flow of nanofluid convince by stretching sheet along convective boundary condition and brought to a conclusion that, Biot number increases the thermal boundary layer thickness remarkably. Ishaket al. [18] examined the consequence of thermal radiation over boundary layer flow of viscous fluid on a moving plate with the help of convective boundary condition. Nadeem et al. [27] and Shaw and Mahanta [22] explored three dimensional hydromagnetic flow of Casson nanofluid and Casson fluid mechanism of convective boundary condition originated by linearly and nonlinearly stretching sheet, respectively. Recently, Oyelakinet al. [30] studied the transfer of heat feature in unstable Casson nanofluid flow by stretching a sheet along convective boundary conditions.

Study of heat transfer is a very essential field of research because its wide range of applications in various engineering and industrial processes such a heat pumps, nuclear reactors cooling, materials processing, rocket thermal ablation and energy production, electronic devices cooling, thermoplastic fabrication, biophysical conduction of heat conduction in tissues. The major disadvantage of the Fourier model [12], is that it cuts down the conservation heat formulation to the energy parabolic equation which displays the medium surveillance as the earliest disturbance. In order to get the better of this difficulty, the term called relaxation time, Cattaneo developed [4] Fourier's law of heat conduction. Christov [6] with finite speed conduction of heat introduced an indifferent formulation for the Maxwell–Cattaneo model. Starzewski- Ostoja [28] characterised the Maxwell–Cattaneo equation of heat flux mathematically by using material time derivatives. Zampoli and Tibullo [37] scrutinised the stability and uniqueness of solutions of incompressible fluid achieved by Cattaneo–Christov heat flux model. Straughan [36] examined numerically the incompressible thermal convection flows. Haddad [14] was examined in detail using a heat flux model with Brinkman porous medium about thermal instability consolidated fluid inertia. Straughan and Ciarletta [7] studied Cattaneo–Christov heat flux equations regarding structural stability and uniqueness. They reported that the solution to a backward in time problem depends continuously on relaxation time. Yilbas and Al-Qahtani [2] employed the Laplace transform method and closed form solution for stress and Cattaneo equation. Papanicolaou et al. [31] examined Cattaneo–Maxwell equations and the impact of thermal relaxation. Han et al. [15] used the Cattaneo–Christov heat flux model for the Maxwell fluids boundary layer flow against the stretching sheet. Mustafa [26] investigated numerically and analytically non-Fourier convection in turning Maxwell fluid flow. He conferred both numerical and analytical solutions and exhibits results of both are in very good concurrence. Bissell [3] applied Cattaneo– Christov heat flux model instead of parabolic Fourier law oscillatory convection flow in a classic Bernard problem to improve the possibility of oscillatory convection. Khan et al. [20] examined HAM procedure for Maxwell fluid boundary layer flow which is reactive chemically with the influence of heat flux model. Raju et al. [32] numerically examined the effect of magneto hydro dynamics over boundary layer flow of a Maxwell non fluid past cylinder underneath heat flux model. They concluded that the coefficient of skin friction is comparatively more in permeable flow on cylinder case in comparison to impermeable flow on cylinder case. Shahid et al. [34] investigated Cattaneo-Christov's heat flux model on radiative Maxwell viscoelastic magnetic flow on stretching permeable sheet. Khan et al. [21] examined upper-convected Maxwell micro polar fluid flow upon semi-infinite stretching surface.

Here, in this work, the evaluation of the effects of boundary layer flow of a Casson fluid along changeable thickness is originated by a stretching sheet by using Cattaneo-Christov heat flux model along with the effects of convective heating and thermal radiation. The more precise numerical solution is obtained by using Keller Box method. These results are discussed graphically for different miscellaneous variables.

2. Mathematical formulation

Consider the two-dimensional incompressible boundary layer flow of Casson fluid over stretching sheet with variable thickness. The velocity of the sheet is supposed to be

$U_m=U_0(x+b)^m$ and it is assumed that the wall thickness of the stretching sheet may increase or decrease with the power index m of the distance from the slot. For m = 1 the problem reduces to flat stretching sheet. The viscosity of the fluid is $\mu=\mu_0 e^{(T-T_0)}$. We used Cattaneo-Christov heat flux model instead of Fourier's law to investigate the heat transfer characteristics.

Physical model of the problem is shown in figure 1.

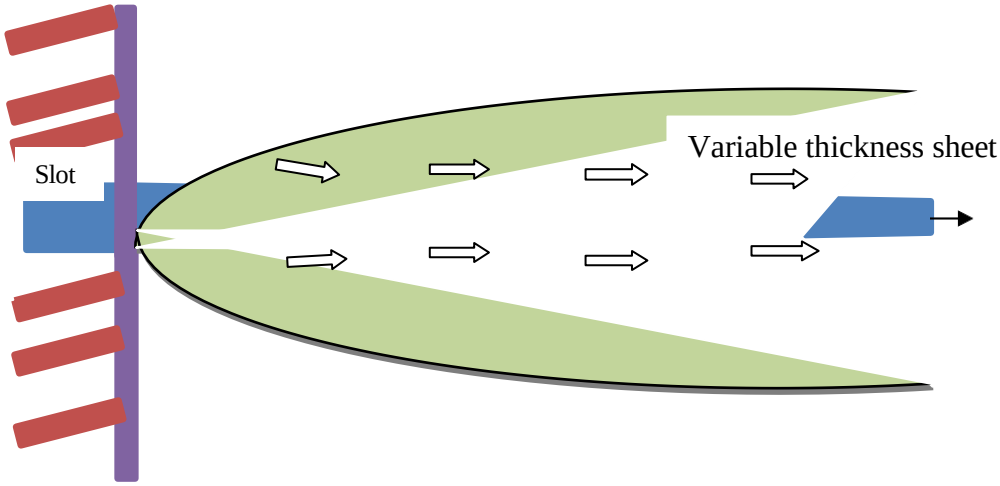

Fig. 1 Stretching sheet variable thickness.

We have

$$\nabla.\bar{U}=0, \tag{1}$$

$$\bar{\rho}\frac{D\bar{U}}{Dt}=\nabla.\tau+\bar{\rho}b, \tag{2}$$

Where $\bar{U}$, $\bar{\rho}$denotes the velocity field, the density of the flow respectively and $b=\bar{J}\times B$is the body force. The Cauchy stress tensor is

$$\tau=\begin{cases}2\left(\mu_B+\dfrac{\bar{P}_z}{\bar{\Psi}}\right)e_{ij}, \bar{\Psi}>\bar{\Psi}_c\\ 2\left(\mu_B+\dfrac{\bar{P}_z}{\sqrt{2\bar{\Psi}}}\right)e_{ji}, \bar{\Psi}<\bar{\Psi}_c\end{cases} \tag{3}$$

Here $\bar{P}_z$, μ_B,$\bar{\Psi}$ are the yield stress of the field, a plastic dynamic viscosity of non-Newtonian fluid, the product of the components of rate deformation respectively. And $\bar{\Psi}=e_{ij}e_{ji}$, e_{ij} is the (i ,j) component of the deformation rate and $\bar{\Psi}_c$ is the critical value of $\bar{\Psi}$ based on non-Newton model. Adding temperature equation to the reformed equations we get

the following equations

$$\frac{\partial u}{\partial x}+\frac{\partial v}{\partial y}=0, \tag{4}$$

$$\bar{u}\frac{\partial \bar{u}}{\partial x}+\bar{v}\frac{\partial \bar{u}}{\partial y}=\frac{\mu}{\rho}\left(1+\frac{1}{\beta}\right)\frac{\partial^2 \bar{u}}{\partial y^2}+\nu\left(1+\frac{1}{\beta}\right)\frac{\partial \bar{u}}{\partial y}\frac{\partial \mu}{\partial y}, \tag{5}$$

$$\rho c_p \bar{U}.\nabla T=-\nabla.q+q_r^*, \tag{6}$$

Here $\bar{u}$ and $\bar{v}$ are the velocity components respectively along x and y-directions, ν and μ are the kinetic viscosity and the variable viscosity, q and q_r^*, are the heat flux and the radiative heat flux, and c_p, T^*, β, the specific heat, the temperature of the fluid, the Casson parameter respectively. From Eq. (3.2.6)

$$q+\bar{\lambda}\left(\frac{\partial q}{\partial t}+\bar{U}.\nabla.q-q.\nabla\bar{U}+(\nabla.\bar{U})q\right)=-\bar{k}\nabla T^*-q_r^*, \tag{7}$$

Where $\bar{\lambda}$ is denotes the thermal relaxation time and $\bar{k}$ is the thermal conductivity of the fluid. Eqs. (6) and (7) together give the following equation

$$\bar{u}\frac{\partial T^*}{\partial x}+\bar{v}\frac{\partial T^*}{\partial y}+$$
$$\bar{\lambda}\left(\bar{u}\frac{\partial \bar{u}}{\partial x}\frac{\partial T^*}{\partial x}+\bar{v}\frac{\partial \bar{v}}{\partial y}\frac{\partial T^*}{\partial y}+\bar{u}\frac{\partial \bar{v}}{\partial x}\frac{\partial T^*}{\partial y}+\bar{v}\frac{\partial \bar{u}}{\partial y}\frac{\partial T^*}{\partial x}+2\bar{u}\bar{v}\frac{\partial^2 T^*}{\partial x\partial y}+\bar{u}^2\frac{\partial^2 T^*}{\partial x^2}+\bar{v}^2\frac{\partial^2 T^*}{\partial y^2}\right)$$
$$=\frac{\bar{k}}{\rho c_p}\frac{\partial^2 T^*}{\partial y^2}-\frac{1}{\rho c_p}\frac{\partial q_r^*}{\partial y}, \tag{8}$$

The boundary conditions are:

$$\bar{u}=U_w(x)=U_0(x+b)^m, \bar{v}=0, \bar{k}\frac{\partial T^*}{\partial y}=-h_f(T_f-T^*) \text{ at } y=A(x+b)^{\frac{1-m}{2}},$$

$$\bar{u}\to 0, T^*\to T_\infty, \text{ as } y\to\infty. \tag{9}$$

The Rosseland approximation for q_r^* is

$$q_r^*=-\frac{4\sigma^*}{3k^*}\frac{\partial T^{*4}}{\partial y} \tag{10}$$

Here σ^* is the Stefan-Boltzmann constant and $k^*$is the mean absorption coefficient.

Using Taylor series expansion for T^*, we have

$$T^{*4} \cong 4T_\infty^3 T^* - 3T_\infty^4 \tag{11}$$

From (10) and (11)

$$q_r^* = -\frac{16\sigma^*}{3k^*} T_\infty^3 \frac{\partial T^*}{\partial y} \tag{12}$$

Considering the following transformations:

$$\eta = \sqrt{\frac{(m+1)U_0(x+b)^{m-1}}{2\nu}}\, y, \psi^* = \sqrt{\frac{2\nu U_0(x+b)^{m+1}}{m+1}}\, \overline{F}(\mu), \overline{u} = U_0(x+b)^m \overline{F}'(\eta),$$

$$\overline{v} = -\sqrt{\frac{(m+1)\nu U_0(x+b)^{m-1}}{2}}\left[\overline{F}(\eta) + \eta\frac{m-1}{m+1}\overline{F}'(\eta)\right], \Theta(\eta) = \frac{T^* - T_\infty}{T_w - T_\infty}. \tag{13}$$

Let $G = 1 + \frac{1}{\beta}$, $1 + \frac{4}{3}\overline{Rd} = A$

The governing equations are reduced to the following equations:

$$G\left(\overline{F}''' - B\Theta'\overline{F}''\right)(1 - B\Theta) + \overline{F}\overline{F}'' - \frac{2m}{m+1}(\overline{F}')^2 = 0, \tag{14}$$

$$\frac{1}{\Pr} A\Theta'' + \overline{F}\Theta' - \gamma\left(\frac{m-3}{2}\overline{F}\overline{F}'\Theta' + \frac{m+1}{2}\overline{F}^2\Theta''\right) = 0, \tag{15}$$

The boundary conditions become

$$\overline{F}(\alpha) = \frac{\alpha(1-m)}{(1+m)}, \overline{F}'(\alpha) = 1, \Theta'(0) = -Bi(1 - \Theta(0)),$$
$$\overline{F}'(\infty) \to 0, \Theta(\infty) \to 0 \tag{16}$$

Where $\alpha = A\sqrt{\frac{U_0(m+1)}{2\nu}}$ denotes the plat surface. In order to make non-dimensional equations, we define $\overline{F}(\zeta) = f(\eta - \alpha) = f(\eta)$ which gives

$$G\left(f''' - B\theta f''\right)(1 - B\theta) + ff'' - \frac{2m}{m+1}(f')^2 = 0, \tag{17}$$

$$\frac{1}{\Pr}A\theta''+f\theta'-\gamma\left(\frac{m-3}{2}ff'\theta'+\frac{m+1}{2}f^2\theta''\right)=0, \tag{18}$$

The boundary conditions become

$$f(0)=\frac{\alpha(1-m)}{(1+m)}, f'(0)=1, \theta'(0)=-Bi(1-\theta(0)),$$
$$f'(\infty)\to 0, \theta(\infty)\to 0 \tag{19}$$

$B=e^{-\zeta(T^*-T_\infty)}$ is the variable viscosity parameter, $\Pr=\frac{\mu c_p}{\bar{k}}$ is the Prandtl number, $Rd=\frac{4\sigma^* T_\infty^3}{\bar{k}k^*}$ is the thermal radiation parameter, $Bi=\frac{h_f}{\bar{k}}\sqrt{\frac{\nu}{U_0}}$ is the Biot number and $\gamma=\lambda U_0(x+b)^{m-1}$ is the thermal relaxation parameters.

The wall shear stress at the sheet is given by

$$\tau_w=\mu G\frac{\partial \bar{u}}{\partial y}, \tag{20}$$

The skin friction can be defined as

$$C_f=\frac{\tau_w}{\sqrt{(m+1)U_0\,2\nu}}(x+b)^{\frac{-(3m-1)}{2}}, \tag{21}$$

The dimensionless forms of skin friction is defined as

$$C_f\sqrt{\mathrm{Re}_x}=\left[G(1-\gamma\theta)f'\right]_{\eta=0}, \text{ Where } \mathrm{Re}_x=\sqrt{\frac{U_0}{\nu}}x. \tag{22}$$

3. Numerical Solution of the Problem

The Equations (17) and (18) with the boundary conditions (Eq. (19)) are solved by using Keller-box method, a very appropriate method for non linear parabolic problems. By substituting new dependent variables, these equations are converted into first-order equations, then central difference expressions are used later Newton's method is applied to linearize this system of nonlinear equations, then transformed into matrix-vector form and then the system is solved by Tri diagonal Block-elimination method. MATLAB software is used for graphical illustrations and tabular values. The grid size is chosen for η as 0.01 and the convergence criterion is less than 0.5×10^{-5}, which is accurate up to four decimals. For different values of η_∞, dual solutions are obtained and they are dependent on the involving parameters. Table.1 shows that the present results are valid and accurate with some restricted cases of Salahuddin et.al. [33] and Wang [39].

We assumed $f'=v,\ v'=\bar{r},\ \bar{s}=\theta',\ t=s^{+}$ And Eqs. (17) and (18) become,

$$G(1-B\theta)(\bar{r}'-B\bar{s}\bar{r})+fr-\frac{2m}{m+1}v^2=0 \tag{23}$$

$$\frac{1}{P_r}A\bar{s}'+f\bar{s}+\gamma\left(\frac{m-3}{2}fv\bar{s}-\frac{m+1}{2}f^2\bar{s}'\right)=0 \tag{24}$$

$$f_j^i-f_{j-1}^i=\frac{h_j}{2}\left[v_j^j+v_{j-1}^j\right] \tag{25}$$

$$v_j^i-v_{j-1}^i=\frac{h_j}{2}\left[\bar{r}_j^i+\bar{r}_{j-1}^i\right] \tag{26}$$

$$\theta_j^i-\theta_{j-1}^i=\frac{h_j}{2}\left[\bar{s}_j^i+\bar{s}_{j-1}^i\right] \tag{27}$$

$$G(1-B\theta)\left[\left(\bar{r}_j^i-\bar{r}_{j-1}^i\right)-h_jBs^i{}_{j-\frac{1}{2}}\bar{r}^i{}_{j-\frac{1}{2}}\right]+h_jf^i{}_{j-\frac{1}{2}}\bar{r}^i{}_{j-\frac{1}{2}}-h_j\left(\frac{2m}{m+1}\right)\left(v^i{}_{j-\frac{1}{2}}\right)^2=P_{j-\frac{1}{2}} \tag{28}$$

$$A\left(\bar{s}_j^i-\bar{s}_{j-1}^i\right)+P_rh_jf^i{}_{j-\frac{1}{2}}\bar{s}^i{}_{j-\frac{1}{2}}+P_rh_j.\gamma\left[\left(\frac{m-3}{2}.f^i{}_{j-\frac{1}{2}}v^j{}_{j-\frac{1}{2}}\bar{s}^i{}_{j-\frac{1}{2}}\right)\right]-\frac{m+1}{2}\left(\bar{s}_j^i-\bar{s}_{j-1}^i\right)f^{i-1}_{j-\frac{1}{2}}=L_{j-\frac{1}{2}} \tag{29}$$

here

$$P_{j-\frac{1}{2}}=-G(1-B\theta)\left[\left(\bar{r}_j^{i-1}-\bar{r}_{j-1}^{i-1}\right)-h_jB\bar{s}^{i-1}_{j-\frac{1}{2}}\bar{r}^{i-1}_{j-\frac{1}{2}}\right]+h_jf^{i-1}_{j-\frac{1}{2}}\bar{r}^{i-1}_{j-\frac{1}{2}}-h_j\left(\frac{2m}{m+1}\right)\left(v^{i-1}_{j-\frac{1}{2}}\right)^2 \tag{30}$$

and

$$L_{j-\frac{1}{2}}=-A\left(\bar{s}_j^{i-1}-\bar{s}_{j-1}^{i-1}\right)+P_rh_jf^{i-1}_{j-\frac{1}{2}}\bar{s}^{i-1}_{j-\frac{1}{2}}+P_rh_j.\gamma\left[\left(\frac{m-3}{2}.f^{i-1}_{j-\frac{1}{2}}v^{i-1}_{j-\frac{1}{2}}\bar{s}^{i-1}_{j-\frac{1}{2}}\right)\right]-\frac{m+1}{2}\left(\bar{s}_j^{i-1}-\bar{s}_{j-1}^{i-1}\right)f^{i-1}_{j-\frac{1}{2}} \tag{31}$$

Boundary conditions are

$$f_0^i=\frac{\alpha(1-m)}{1+m},\ v_0^i=1,\ v_J^i=0,\ t_0^i=1,\ t_J^i=0 \tag{32}$$

Newton's method:

$$f_j^{i+1} = f_j^i + \bar{\delta} f_j^i \tag{33}$$

Similarly, for $v, \bar{r}, \bar{s}$ and t, we get

$$\left(\bar{\delta} f_j - \bar{\delta} f_{j-1}\right) - \frac{h_j}{2}\left(\bar{\delta} v_j + \bar{\delta} v_{j-1}\right) = \left(\bar{l}_1\right)_j \tag{34}$$

$$\left(\bar{\delta} v_j - \bar{\delta} v_{j-1}\right) - \frac{h_j}{2}\left(\bar{\delta} r_j + \bar{\delta} r_{j-1}\right) = \left(\bar{l}_2\right)_j \tag{35}$$

$$\left(\bar{\delta}\theta_j - \bar{\delta}\theta_{j-1}\right) - \frac{h_j}{2}\left(\bar{\delta} s_j + \bar{\delta} s_{j-1}\right) = \left(\bar{l}_3\right)_j \tag{36}$$

$$(C_1)_j \bar{\delta} r_j + (C_2)_j \bar{\delta} r_{j-1} + (C_3)_j \bar{\delta} v_j + (C_4)_j \bar{\delta} v_{j-1} + (C_5)_j \bar{\delta} f_j + (C_6)_j \bar{\delta} f_{j-1} = \left(\bar{l}_4\right)_j \tag{37}$$

$$(d_1)_j \bar{\delta} s_j + (d_2)_j \bar{\delta} s_{j-1} + (d_3)_j \bar{\delta} v_j + (d_4)_j \bar{\delta} v_{j-1} + (d_5)_j \bar{\delta} f_j + (d_6)_j \bar{\delta} f_{j-1} = \left(\bar{l}_5\right)_j \tag{38}$$

here

$$(C_1)_j = G(1 - B\theta) + \frac{h_j f_{j-\frac{1}{2}}}{2} - \frac{B h_j}{2} \bar{s}^i_{j-\frac{1}{2}} \tag{39}$$

$$(C_2)_j = -G(1 - B\theta) + \frac{h_j f^i_{j-\frac{1}{2}}}{2} - \frac{B h_j}{2} \bar{s}^i_{j-\frac{1}{2}} \tag{40}$$

$$(C_3)_j = -\frac{m h_j}{m+1} . v^i_{j-\frac{1}{2}} \tag{41}$$

$$(C_4)_j = (C_3)_j \tag{42}$$

$$(C_5)_j = \frac{h_j \bar{r}^i_{j-\frac{1}{2}}}{2} \tag{43}$$

$$(C_6)_j = (C_5)_j \tag{44}$$

$$(d_1)_j = A + \frac{P_r h_j f_{j-\frac{1}{2}}}{2} + P_r h_j \gamma \left(\frac{m-3}{4}\right) f_{j-\frac{1}{2}} v_{j-\frac{1}{2}} - P_r \gamma \left(\frac{m+1}{2}\right) f^2_{j-\frac{1}{2}}$$

$$(d_2)_j = -A + \frac{P_r h_j f_{j-\frac{1}{2}}}{2} + P_r h_j \gamma \left(\frac{m-3}{4}\right) f_{j-\frac{1}{2}} v_{j-\frac{1}{2}} - P_r \gamma \left(\frac{m+1}{2}\right) f^2_{j-\frac{1}{2}}$$

$$(d_3)_j = \frac{m-3}{4} P_r h_j \gamma f^i_{j-\frac{1}{2}} \bar{s}^i_{j-\frac{1}{2}}$$

(45)

$$(d_4)_j = (d_3)_j$$

$$(d_5)_j = P_r h_j \bar{s}^i_{j-\frac{1}{2}} + P_r h_j \gamma \left(\frac{m-3}{4}\right) \bar{s}^i_{j-\frac{1}{2}} v^i_{j-\frac{1}{2}} - P_r h_j \gamma \left(\frac{m+1}{4}\right) f_{j-\frac{1}{2}} \bar{s}^i_{j-\frac{1}{2}}$$

$$(d_6)_j = (d_5)_j$$

$$A\delta = l$$

$$A\delta = l$$

Here

$$l = \begin{bmatrix} \bar{l}_1 \\ \bar{l}_2 \\ \vdots \\ \bar{l}_J \end{bmatrix}, \quad \delta = \begin{bmatrix} \delta^1 \\ \vdots \\ \delta_J \end{bmatrix} \tag{46}$$

$$A = \begin{bmatrix} E_1 & C_1 & & & \\ B_1 & E_2 & C_2 & & \\ & & B_{J-1} & E_{j-1} & C_{j-1} \\ & & & B_{J-1} & A_J \end{bmatrix} \tag{47}$$

And

$$\delta_1 = \begin{bmatrix} \delta r_0 \\ \delta s_0 \\ \delta f_1 \\ \delta r_1 \\ \delta s_1 \end{bmatrix}, \quad \delta_j = \begin{bmatrix} \delta v_1 \\ \delta \theta_1 \\ \delta f_2 \\ \delta r_2 \\ \delta s_2 \end{bmatrix} \tag{48}$$

$$[E_1] = \begin{bmatrix} 0 & 0 & 1 & 0 & 0 \\ \frac{-h_1}{2} & 0 & 0 & \frac{-h_1}{2} & 0 \\ 0 & \frac{-h_1}{2} & 0 & 0 & \frac{-h_1}{2} \\ c_2 & 0 & c_5 & c_1 & 0 \\ 0 & d_2 & d_5 & 0 & d_1 \end{bmatrix} \tag{49}$$

$$C = \begin{bmatrix} \frac{-h_1}{2} & 0 & 0 & 0 & 0 \\ 1 & 0 & 0 & 0 & 0 \\ 0 & 1 & 0 & 0 & 0 \\ c_3 & 0 & 0 & 0 & 0 \\ d_3 & 0 & 0 & 0 & 0 \end{bmatrix} \tag{50}$$

$$E_2 = \begin{bmatrix} \frac{-h_2}{2} & 0 & 1 & 0 & 0 \\ -1 & 0 & 0 & \frac{-h_2}{2} & 0 \\ 0 & -1 & 0 & 0 & \frac{-h_2}{2} \\ c_4 & 0 & c_5 & c_1 & 0 \\ d_4 & 0 & d_5 & 0 & d_1 \end{bmatrix} \tag{51}$$

$$B = \begin{bmatrix} 0 & 0 & -1 & 0 & 0 \\ 0 & 0 & 0 & \frac{-h_2}{2} & 0 \\ 0 & 0 & 0 & 0 & \frac{-h_2}{2} \\ 0 & 0 & c_6 & c_2 & 0 \\ 0 & 0 & d_6 & 0 & d_2 \end{bmatrix} \tag{52}$$

4. Results and Discussions

Numerical examinations are done comprehensively to analyse the temperature distribution and velocity field within the boundary layer by considering both the wall temperature gradient and wall velocity gradient. We can see their changes for different parameters like Bi, β, Pr , γ, B , Rd , m , α from the Figures 2 – 11. The values of these parameters are chosen as Bi = 0.2, β= 2, Pr =0.71, γ= 0.2, B = 0.4, Rd = 0.5, m = 0.1, α=0.1.

Fig. 2 explores the influence of Casson factor β on fluid velocity f'. It's observed that there is an inverse relationship highlighting the impact of β on the physical system, demonstrating how an increase in β leads to a reduction in f'

The Casson factor is demonstrate as $\beta = \frac{\mu_B \sqrt{2\overline{\psi}_c}}{\overline{P}_y}$. Here $\overline{\psi}_c$ is the critical value of $\overline{\psi}$ it is the product of rate of deformation with itself, μ_B is dynamic viscosity, and $\overline{P}_y$ is fluid's yield stress. It's easy to understand from the equation that Casson parameter, dynamic viscosity is directly proportional to each other. Hence, increase in the value of β implies an increase in plastic dynamic viscosity μ_B, which indicates more resistance to the flow of fluid hence the result.

Figure 3, highlights how Casson fluid factor β influences the heat transfer characteristics, it is directly proportional to temperature distributions. The reason behind such increase is that the movement of Casson factor leads to decrease in the fluid velocity, Consequently, when the fluid is further dragged against physical boundaries, energy is lost, leading to an increase in the fluid temperature within the boundary layer. This enhancement in temperature is a direct result of the viscous dissipation of energy as the fluid flows.

Figures 4 and 6, shows that for m<1, an increase in the wall thickness factor leads to a decrease in the velocity at any point near the plate. However, for m>1, the situation is reversed, where an increase in the wall thickness factor results in an increase in velocity near the plate. Furthermore, it is evident from the figures that for larger values of α, when m<1, the boundary layer thickness becomes thinner, while for larger values of α when m>1, the boundary layer thickness becomes thicker.

Figures 5 and 7 display the wall thickness factor reduces the thermal boundary layer thickness and increases the heat transfer rate when m<1, but the opposite effect is observed when m>1. Physically, increased value of α when m<1 reduces the velocity of the flow. This occurs because when the wall thickness varies, not all of the pulling force from the stretching sheet is transmitted to the fluid, leading to a reduction in both the temperature distribution and the friction between fluid layers. However, when m>1, the velocity of the flow layers increases, which raises the frictional forces between the layers and consequently increases the temperature. Moreover, for higher values of α, the thermal boundary layer becomes thinner when m<1 compared to m>1.

In fig (8) shows the impact of Bi on temperature profile. perceive that temperature enhances

when Bi increases. Aziz and Makinde [93] explored the similar outcome like Biot number describe that the ratio of hot fluid side to the cold fluid side convection resistances upon the surface. Furthermore, the hot fluids thermal resistance is proportional to h_f, hence increasing Bi values leads to increase side convection of hot fluid. Consequently, thickness of thermal boundary layer increases.

Fig 9 displays the consequences of non-dimensional thermal relaxation time γ over temperature profiles. It is noticed that temperature and thermal relaxation time are inversely proportional to each other. Furthermore, it is observed that. In both cases Maxwell and Newtonian, change in temperature by thermal relaxation of time is of same magnitude. For $\gamma = 0$ the temperature profile is greater for Fourier's law with respect to Cattaneo–Christov model.

Figure 10 illustrates the temperature distributions of the variable η for dissimilar values of the thermal radiation factors. From figure, it is clearly noticed that by increasing the value of the thermal radiation factor, the surface temperature $\theta(0)$, thickness of thermal boundary layer, temperature distribution all increases. The reason behind this is the radiative heat flux increases when Rosseland radiative absorptive decreases which further, displays an increase radiative heat transfer rate to the fluid, results the rise in fluid temperature. With this certainty, the influence of radiation becomes greater noteworthy as Rd→∞ and the influence of radiation ignored when Rd = 0.

Figure 11 shows the effects of the Prandtl number (Pr) on the temperature profile. It is evident that as the Prandtl number increases, the temperature near the wall decreases. An increase in the Prandtl number leads to a reduction in the thermal boundary layer thickness, indicating that heat diffuses more rapidly than momentum. Consequently, thermal diffusivity exceeds momentum diffusivity. As Pr increases, the temperature profile is compressed closer to the wall. This behavior is particularly pronounced when Pr << 1, where the fluid is more conductive, allowing heat from the sheet to transfer more rapidly compared to fluids with higher Pr values. Therefore, the Prandtl number is essential for enhancing the rate of cooling in conductive flows.

Figure 12 -15 illustrate the effects of wall thickness factor, magnetic factor, variable viscosity factor, and Casson fluid factor on the coefficients of skin friction and Nusselt number. It is evident that an increase in the Casson fluid factor results in a decrease in both the coefficient of local skin friction and the Nusselt number. Similarly, while increasing the magnetic factor leads to a decrease in the local Nusselt number but the coefficient of skin friction increases. Furthermore, an enhancement in the variable viscosity parameter causes a reduction in both the coefficient of skin friction and the Nusselt number. Conversely, increasing the wall thickness factor results in an enhancement of both the coefficient of skin friction and the Nusselt number.

5. Conclusions: Key Findings of the present study:

- Casson Fluid Parameter Impact: An increase in the Casson fluid parameter leads to a deceleration of the fluid over the sheet.

➢ Cattaneo-Christov Model Comparison: The behaviour of factors in the Cattaneo-Christov model aligns qualitatively with those in Fourier's heat conduction law.

➢ Effect of Relaxation Time and Velocity Power Index: The thickness of the thermal boundary layer and temperature exhibits a decreasing trend with relaxation time. Similarly, an increase in the velocity power index parameter causes the fluid to slow down over the stretching sheet.

➢ Influence of Prandtl Number and Radiation: Both the thickness of the thermal boundary layer and temperature decrease with Prandtl number, while the radiation factor acts oppositely.

➢ Casson Fluid Factor Impact: Increasing the Casson fluid factor results in a simultaneous decrease in both the coefficient of drag skin friction and heat transfer values.

➢ These findings provide valuable insights for researchers in diverse fields, serving as a reference for understanding the physics of flow past a stretching sheet and contributing to advancements in scientific and engineering applications.

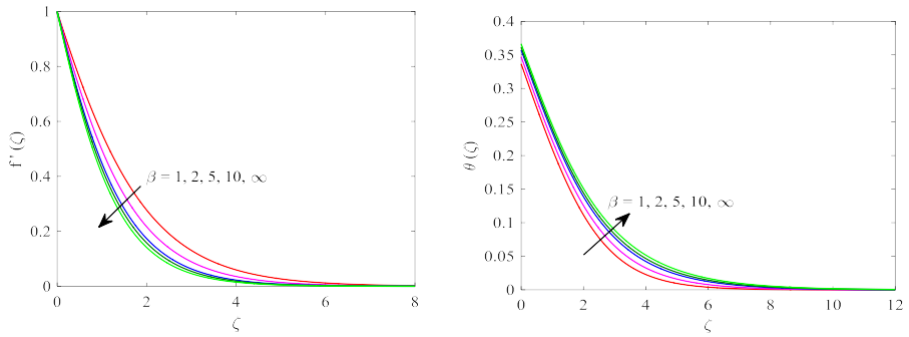

Figure 2 & 3 Dimensionless velocity and temperature distributions $f'(\zeta)$ and $\theta(\zeta)$ for different values of β

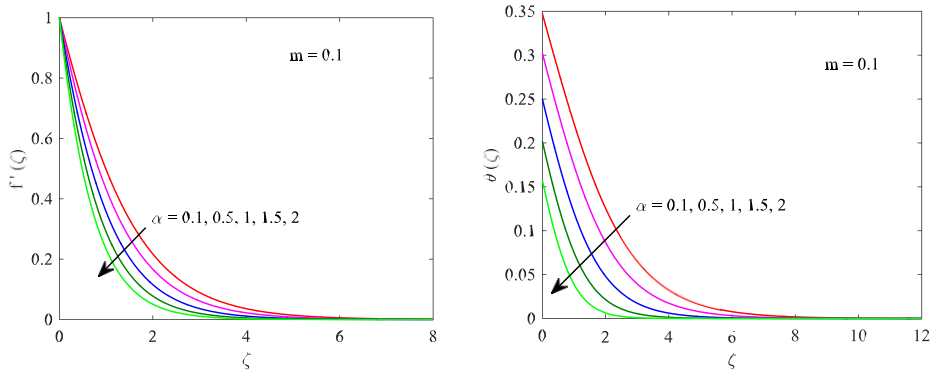

Figure 4 & 5: Dimensionless velocity and temperature distributions $f'(\zeta)$ and $\theta(\zeta)$ for different values of α for m <1.

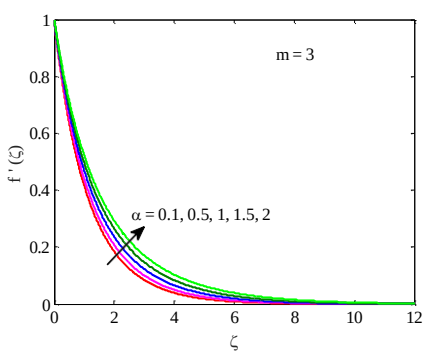

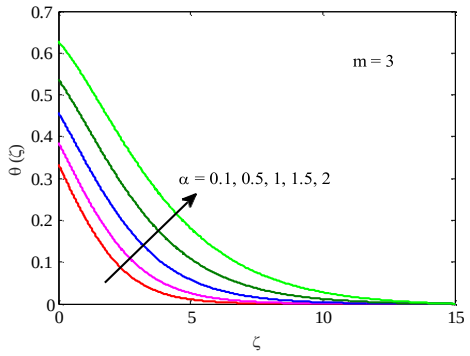

Figure 6 & 7: Dimensionless velocity and temperature distributions $f'(\zeta)$ and $\theta(\zeta)$ for different values of α for m>1.

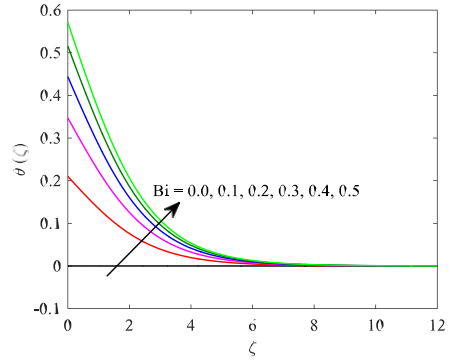

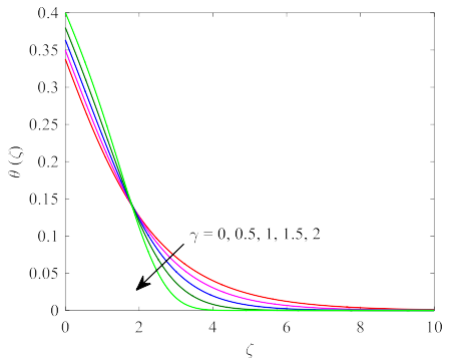

Figure 8 & 9: Dimensionless temperature distribution $\theta(\zeta)$ for different values of Bi, γ.

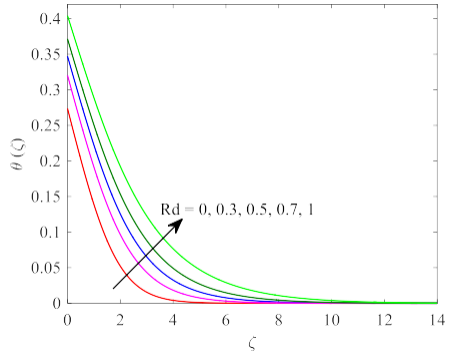

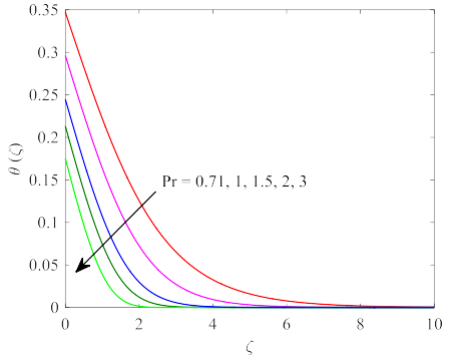

Figure 10 & 11: Dimensionless temperature distribution $\theta(\zeta)$ for different values of Rd, Pr.

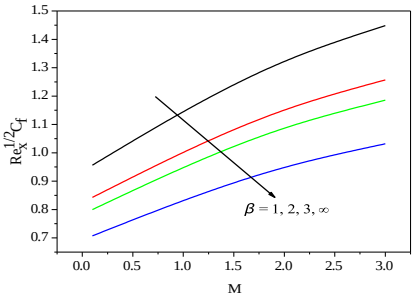

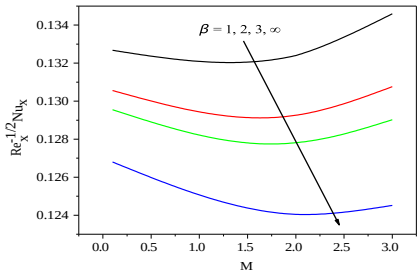

Figure 12 & 13: Skin friction coefficient $\mathrm{Re}_x^{1/2} C_f$ and Local Nusselt number $\mathrm{Re}_x^{-1/2} Nu_x$ for different values of M &β.

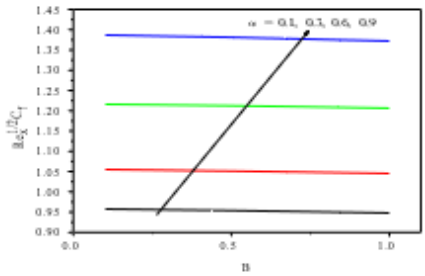

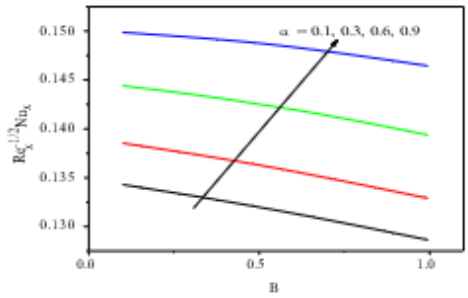

Figure 14 & 15: Skin friction coefficient $\mathrm{Re}^{1/2} C$ and Local Nusselt number $\mathrm{Re}^{-1/2} Nu$

Table 1: Computation of $-\theta'(0)$ for different values of Prandtl number Pr when $\gamma=\beta=a$ =Rd = 0 but m = 1.

Pr	Salahuddin et al. [146]	Wang et al. [161]	Present Results
0.07	0.0654	0.0656	0.065623
0.20	0.1688	0.1691	0.169089
0.70	0.4535	0.4539	0.453916
2.00	0.9108	0.9114	0.911358
7.00	1.8944	1.8954	1.895403
20.00	3.3522	3.3539	3.353904
70.00	6.4619	6.4622	6.462200

References

1. Ali, M.E., (1994), Heat transfer characteristics of a continuous stretching surface, Warme - Und Stoffubertragung, Vol.29, pp.227-234.
2. Al-Qahtani, H. and Yilbas, B.S., (2010), The closed form solutions for Cattaneo and stress equations due to step input pulse heating, Phys B., Vol. 405(18), pp.3869-3874.
3. Bissell, J.J., (2015), On oscillatory convection with the Cattaneo- Christov hyperbolic heat- flow model, Proc R Soc A.,Vol.471:20140845
4. Cattaneo,C.,(1948),Sulla conduzionedelcalore, Atti del Seminario Maermatico e Fisico dell Universita di Modena e Reggio Emilia, Vol. 3, pp. 83-101.
5. Chen, T.S,, Ali, M.M. and Armaly, B.F., (1984), Natural convection-radiation interaction in boundary layer flow over horizontal surfaces, AIAA Journal, Vol.22(12), pp.1797-1803.
6. Christov, C.I., (2009), On frame indifferent formulation of the Maxwell–Cattaneo model of finite-speed heat conduction, Mech Res Commun., Vol.36(4), pp.481-486.
7. Ciarletta, M. and Straughan, B., (2010), Uniqueness and structural stability for the Cattaneo- Christov equations, Mech Res Commun., Vol. 37(5), pp.445-447.
8. Cortell, R., (1970), Viscous flow and heat transfer over a nonlinearly stretching sheet, Appl. Math. Comput., Vol. 184, pp.864-873.
9. Crane, L.J., (1970), Flow past a stretching plate, Z. Angew. Math. Phys., Vol.21, pp.645-647.
10. Elbashbeshy, E.M.A., (2000), Radiation effect on heat transfer over a stretching surface. Canadian Journal of Physics, Vol.78 (12), pp.1107-1112.
11. Eldabe, N.T.M. and Salwa, M.G.E., (1995), Heat transfer of MHD non-Newtonian Casson fluid flow between two rotating cylinders, J. Phys. Soc. Jpn., Vol.64, pp.41-64.
12. Fourier, J.B.J., (1822), Theorieanalytique de la chaleur. English translation: The analytic theory of heat (1878). FirmanDidot, Paris.
13. Gupta, P.S. and Gupta, A.S., (1977), Heat and mass transfer on a stretching sheet with suction or blowing, Can. J. Chem. Eng., Vol.55, pp.744-746.
14. Haddad, S.A.M., (2014), Thermal instability in Brinkman porous media with Cattaneo– Christov heat flux, Int J Heat Mass Transf., Vol. 68, pp.659-668.
15. Han, S.H., Zheng, L.C., Li, C.R. and Zhang, X.X., (2014), Coupled flow and heat transfer in viscoelastic fluid with Cattaneo-Christov heat flux model, Appl. Math. Lett., Vol.38, pp 87- 93.
16. Hayat, T., Abbas, Z., Sajid, M. and Asghar, S., (2007), The influence of thermal radiation on MHD flow of a second grade fluid, Int. J. Heat Mass Transf., Vol. 50, pp.931-941.
17. Hayat, T., Nawaz, M., Sajid, M. and Asghar, S., (2009), The effect of thermal radiation on the flow of a second grade fluid, Computers and Mathematics with Applications (Oxford, England), Vol. 58(2), pp.369-379.
18. Ishak, A., Yacob, N. A. and Bachok, N., (2011), Radiation effects on the thermal boundary layer flow over a moving plate with convective boundary condition, Meccanica, Vol.46, pp.795-801.
19. Kechil, S.A. and Hashim, I., (2009), Flow and diffusion of chemically reactive species over a nonlinearly stretching sheet immersed in a porous medium, J. Porous Media, Vol.12, pp.1053- 1063.

20. Khan, M.I., Waqas, M., Hayat, T., Khan, M.I. and Alsaedi, A., (2017), Chemically reactive flow of upper-convected Maxwell fluid with Cattaneo–Christov heat flux model, J Braz. Soc. Mech. Sci. Eng., Vol.39 (11), pp.4571-4578.
21. Khan, S.M., Hammad, M., Batool, S. and Kaneez, H., (2017), Investigation of MHD effects and heat transfer for the upper-convected Maxwell (UCM-M) micropolar fluid with Joule heating and thermal radiation using a hyperbolic heat flux equation, Eur. Phys. J. Plus, Vol.132: 158, DOI 10.1140/epjp/i2017-11428-6
22. Mahanta, G. and Shaw, S., (2015), 3D Casson fluid flow past a porous linearly stretching sheet with convective boundary condition, Alexandria Eng. J., Vol.54, pp.653-659.
23. Makinde, O.D. and Aziz, A., (2011), Boundary layer flow of a nanofluid past a stretching sheet with a convective boundary condition, International Journal of Thermal Sciences, Vol. 50 (7), 2011, pp.1326-1332.
24. Mukhophadhyay, S. and Vajravelu, K., (2013), Diffusion of chemically reactive species in Casson fluid flow over an unsteady permeable stretching surface, J. Hydrodyn., Vol. 25, pp.591-598.
25. Mukhophadhyay, S., (2013), Casson fluid flow and heat transfer over a nonlinearly stretching surface, Chin. Phys. B, Vol.22, 074701.
26. Mustafa, M., (2015), Cattaneo–Christov heat flux model for rotating flow and heat transfer of upper convected Maxwell fluid, AIP Adv, Vol.5(4):047109.
27. Nadeem, S., Haq, R.U. and Akbar, N. S., (2014), MHD three-dimensional boundary layer flow of Casson nanofluid past a linearly stretching sheet with convective boundary condition, IEEE Trans. Nanotechnol., Vol.13, pp.1326-1332.
28. Ostoja-Starzewski, M., (2009), A derivation of the Maxwell-Cattaneo equation from the free energy and dissipation potentials, Int J Eng Sci., Vol. 47(7), pp.807-810.
29. Ouaf, M.E.M., (2005), Exact solution of thermal radiation on MHD flow over a stretching porous sheet, Applied Mathematics and Computation, Vol.170(2), pp.1117-1125.
30. Oyelakin, I.S., Mondal, S. and Sibanda, P., (2016), Unsteady Cassonnanofluid flow over a stretching sheet with thermal radiation, convective and slip boundary conditions, Alexandria Eng. J. Vol.55, pp.1025-1035.
31. Papanicolaou, N.C., Christov, C.I. and Jordan, P.M., (2011), The influence of thermal relaxation on the oscillatory properties of two-gradient convection in a vertical slot, Eur J Mech B/Fluids, Vol. 30(1), pp.68-75.
32. Raju, C.S.K., Sanjeevi, P., Raju, M.C., Ibrahim, S.M., Lorenzini, G. E. and Lorenzini, E., (2017), The flow of magnetohydrodynamic Maxwell nanofluid over a cylinder with Cattaneo– Christov heat flux model, Continuum Mech. Thermodyn., Vol. 29 (6), pp.1347-1363.
33. Salahuddin, T., Malik, M.Y., Hussain, A., Bilal, S. and Awais, M., (2016), MHD flow of Cattaneo–Christov heat flux model for Williamson fluid over a stretching sheet with variable thickness: using numeri-cal approach, J. Magn. Magn. Mater., Vol.401, pp.991-997.
34. Shahid, A., Bhatti, M.M., Anwar Be´g, O. and Kadir, A., (2018), Numerical study of radiative Maxwell viscoelastic magnetized flow from a stretching permeable sheet with the Cattaneo– Christov heat flux model, Neural Comput and Applic, Vol. 30(1), pp.3467-3478.

35. Shehzad, S.A., Hayat, T., Qasim, M. and Asghar, S., (2013), Effects of mass transfer on MHD flow of a Casson fluid with chemical reaction and suction, Braz. J. Chem. Eng., Vol.30, pp.187- 195.
36. Straughan, B., (2010), Thermal convection with the Cattaneo– Christov model, Int J Heat Mass Transf., Vol. 53(1), pp.95-98.
37. Tibullo, V. and Zampoli, V., (2011), A uniqueness result for the Cattaneo - Christov heat conduction model applied to incompressible fluids, Mech Res Commun., Vol.38(1), pp.77-79.
38. Viskanta, R. and Grosh, R.J., (1962), Boundary layer in thermal radiation absorbing and emitting media. International Journal of Heat and Mass Transfer, Vol. 5(9), pp.795-806.
39. 15. Wang, C.Y., (1989), Free convection on a vertical stretching surface with suction and blowing, Appl.Math. Mech., Vol.69, pp.418-420.